

A Josephson Quantum Electron Pump

F. Giazotto,^{1,*} P. Spathis,¹ S. Roddaro,¹ S. Biswas,¹ F. Taddei,¹ M. Governale,² and L. Sorba¹

¹*NEST, Istituto Nanoscienze-CNR and Scuola Normale Superiore, Piazza S. Silvestro 12, I-56127 Pisa, Italy*

²*School of Chemical and Physical Sciences and MacDiarmid Institute for Advanced Materials and Nanotechnology, Victoria University of Wellington, P.O. Box 600, Wellington 6140, New Zealand*

A macroscopic fluid pump works according to the law of Newtonian mechanics and transfers a large number of molecules per cycle (of the order of 10^{23}). By contrast, a nano-scale charge pump can be thought as the ultimate miniaturization of a pump, with its operation being subject to quantum mechanics and with only few electrons or even fractions of electrons transferred per cycle. It generates a direct current in the absence of an applied voltage exploiting the time-dependence of some properties of a nano-scale conductor. The idea of pumping in nanostructures was discussed theoretically a few decades ago [1–4]. So far, nano-scale pumps have been realised only in system exhibiting strong Coulombic effects [5–12], whereas evidence for pumping in the absence of Coulomb-blockade has been elusive. A pioneering experiment by Switkes et al. [13] evidenced the difficulty of modulating in time the properties of an open mesoscopic conductor at cryogenic temperatures without generating undesired bias voltages due to stray capacitances [14, 15]. One possible solution to this problem is to use the ac Josephson effect to induce periodically time-dependent Andreev-reflection amplitudes in a hybrid normal-superconducting system [16]. Here we report the experimental detection of charge flow in an unbiased InAs nanowire (NW) embedded in a superconducting quantum interference device (SQUID). In this system, pumping may occur via the cyclic modulation of the phase of the order parameter of different superconducting electrodes. The symmetry of the current with respect to the enclosed magnetic flux [17, 18] and bias SQUID current is a discriminating signature of pumping. Currents exceeding 20 pA are measured at 250 mK, and exhibit symmetries compatible with a pumping mechanism in this setup which realizes a Josephson quantum electron pump (JQEP).

The microscopic mechanism that enables the transport properties of the NW to be affected by the phases of the superconducting order parameter is Andreev reflection [19]. This is the quantum process for which an electron impinging from the normal side onto the interface between a normal metal and a superconductor, is retro-reflected as a hole (i.e., a time-reversed electron) which picks up the phase of the superconducting order param-

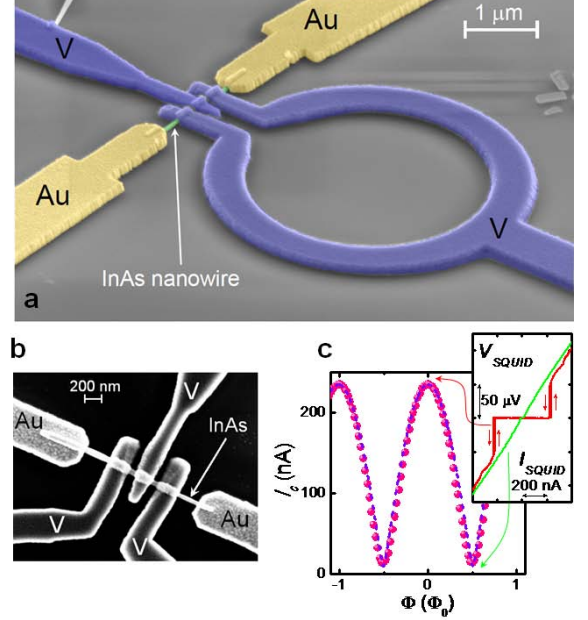


FIG. 1. InAs Josephson quantum electron pump. (a) Pseudo-color scanning electron micrograph of a JQEP. An InAs nanowire (NW) is connected to three ≈ 250 -nm-wide V/Ti superconducting contacts forming two ≈ 50 -nm-long Josephson weak-links and realizing a superconducting quantum interference device (SQUID). Two Au/Ti leads, placed at relative distance of $\approx 1.5 \mu\text{m}$, are contacted to the ends of the NW to allow current detection. The structure was fabricated with electron-beam lithography and evaporation of metals. The normal-state resistance of the SQUID is $\sim 250 \Omega$ whereas that of the Au/NW/Au line is $\sim 3.5 \text{ k}\Omega$. (b) Blow-up of the device core showing the two V/InAs/V Josephson junctions as well as the two Au electrodes. (c) Inset: SQUID voltage (V_{SQUID}) versus current (I_{SQUID}) characteristics at $\Phi = 0$ and $\Phi = \Phi_0/2$ (Φ is the applied magnetic flux whereas Φ_0 is the flux quantum) showing a maximum critical current of $\sim 235 \text{ nA}$. Φ_0 corresponds to a magnetic field of $\approx 1.4 \text{ Oe}$ applied through an effective loop area of $\approx 14.6 \mu\text{m}^2$. Main panel: Φ -dependent modulation of the SQUID critical current I_c . Dashed line is the theoretical behavior of a tunnel and resistively-shunted junction SQUID assuming an asymmetry of $\sim 4\%$ between the critical currents of the two weak-links. Data in (c) are taken at $T = 250 \text{ mK}$.

eter. When two or more superconductors are connected to the NW, multiple Andreev scattering processes can occur between them so that transport through the NW will depend on the differences between the phases of the order parameters [20].

The physical realization of this scheme is shown in Fig. 1a and consists of a heavily-doped InAs semiconducting NW on top of which three fingers of superconducting (S) vanadium (V) are deposited thus implementing a SQUID [21]. Two Au normal-metal electrodes (N) are coupled to the ends of the NW to allow detection of the current I_{wire} flowing through the wire. A close-up of the device core is shown in Fig. 1b. Time-dependence, and possibly pumping, arises from biasing the loop with a current I_{SQUID} larger than the critical current I_c of the SQUID so that the phase differences $\varphi_1(t)$ and $\varphi_2(t)$ across the two Josephson junctions cycle in time at the Josephson frequency $\nu_J = V_{SQUID}/\Phi_0$, where V_{SQUID} is the voltage developed across the SQUID and $\Phi_0 \simeq 2 \times 10^{-15}$ Wb is the flux quantum. In addition, $\varphi_1(t)$ and $\varphi_2(t)$ can be shifted by a constant term $\delta\varphi = 2\pi\Phi/\Phi_0$ originating from an applied magnetic flux Φ threading the loop. This scheme has the advantage that no high-frequency signal needs to be brought to the sample thus simplifying the setup and minimizing the impact of stray capacitances: the time-dependent signal is self-generated thanks to the ac Josephson effect.

Below the critical temperature of the superconductors ($T_c \simeq 4.65$ K) a Josephson current flows through the SQUID across the NW. The SQUID voltage-current characteristics at 250 mK is shown in the inset of Fig. 1c for two representative values of Φ . Whereas for $\Phi = 0$ the characteristic shows a clear dissipationless regime with a critical current $I_c \simeq 235$ nA, for $\Phi = \Phi_0/2$ it behaves almost linearly with I_c largely suppressed. The full $I_c(\Phi)$ dependence (main panel of Fig. 1c) shows the characteristic pattern of a superconducting interferometer. The theoretical curve of a conventional (i.e., described by the RSJ model) SQUID [22] is shown for a comparison (dashed line, see Supplementary Information).

Figure 2a shows a sketch of the pumping measurement setup. A dc current I_{SQUID} is fed through the SQUID terminals while the voltage drop V_{SQUID} is measured against Φ . The N electrodes are grounded and I_{wire} is sensed with an amperometer. The N and S parts of the circuit have no common ground therefore preventing any direct net charge transfer from the SQUID to the NW.

In the following we will concentrate our attention on the symmetries in Φ and I_{SQUID} displayed by the measured signal, as these are of crucial importance for the interpretation of the experiment. The low-temperature SQUID flux-to-voltage transfer function $\mathcal{V}_{SQUID} = \partial V_{SQUID}/\partial\Phi$ versus Φ and I_{SQUID} is displayed in Fig. 2b. In particular, \mathcal{V}_{SQUID} is a Φ_0 -periodic function of Φ and is *antisymmetric* in Φ and I_{SQUID} . By contrast, the flux-to-current transfer function of the NW, $\mathcal{I}_{wire} = \partial I_{wire}/\partial\Phi$ (Fig. 2c), besides exhibiting the same Φ_0 -periodicity shows a drastically different behavior, being almost *symmetric* either in Φ or in I_{SQUID} . A similar behavior with the same symmetries of \mathcal{I}_{wire} is displayed by the NW flux-to-voltage transfer function,

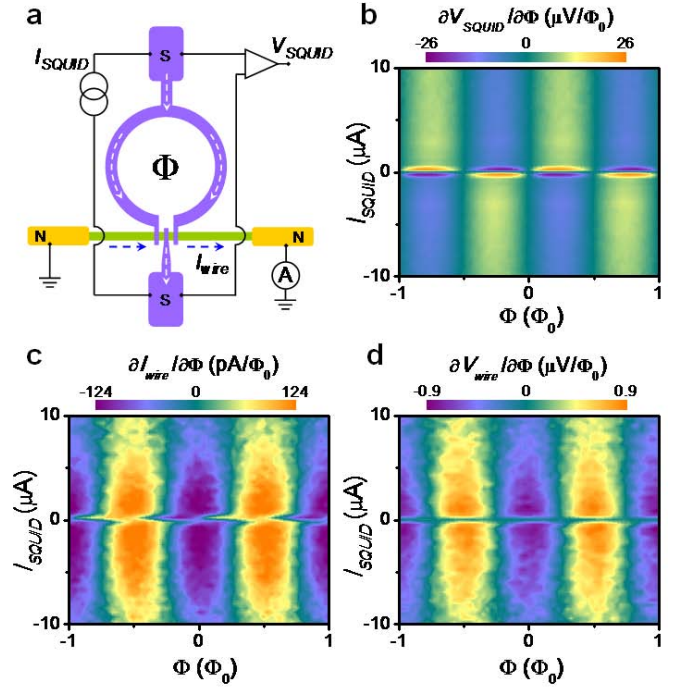


FIG. 2. Experiment setup and transfer functions characteristics. (a) Schematic drawing of the JQEP setup. A dc current I_{SQUID} is fed into the SQUID terminals through a floating source while the voltage drop V_{SQUID} is recorded against the applied magnetic flux Φ threading the ring. When I_{SQUID} exceeds the SQUID critical supercurrent the ac Josephson effect sets up inducing a current I_{wire} which flows in the NW. I_{wire} is sensed through an amperometer. S and N denote superconductors and normal metals, respectively. (b) Color plot of the SQUID flux-to-voltage transfer function $\mathcal{V}_{SQUID} = \partial V_{SQUID}/\partial\Phi$ versus Φ and I_{SQUID} . \mathcal{V}_{SQUID} is antisymmetric in Φ and I_{SQUID} . (c) Color plot of the NW flux-to-current transfer function $\mathcal{I}_{wire} = \partial I_{wire}/\partial\Phi$ versus Φ and I_{SQUID} . (d) Color plot of the NW flux-to-voltage transfer function $\mathcal{V}_{wire} = \partial V_{wire}/\partial\Phi$ versus Φ and I_{SQUID} . Data are taken with a voltmeter in an open-circuit configuration, i.e., without allowing I_{wire} to flow. Note the markedly different behavior displayed by \mathcal{I}_{wire} and \mathcal{V}_{wire} which are almost symmetric in Φ as well as in I_{SQUID} . All measurements are taken at $T = 250$ mK with low-frequency phase-sensitive technique to get higher sensitivity and reduced noise.

$\mathcal{V}_{wire} = \partial V_{wire}/\partial\Phi$ (Fig. 2d), where V_{wire} is measured with open NW contacts. \mathcal{I}_{wire} and \mathcal{V}_{wire} result from different but complementary measurements, and the evidence of such a similarity suggests that both reflect the same physical mechanism (see Supplementary Information). As we shall argue, the nature of the symmetries displayed by \mathcal{I}_{wire} and \mathcal{V}_{wire} is compatible with a quantum pumping mechanisms.

In general, the pumped current is not expected to show definite parity with Φ [17, 18], therefore I_{wire} can have a flux-symmetric component as well. This, however, could be ascribed also to other mechanisms than pumping. In

addition, I_{wire} is even not expected to possess any definite parity with I_{SQUID} . In order to extract a pure pumped current contribution from the whole measured signal we focus on the component of I_{wire} which is *antisymmetric* in Φ , I_{wire}^A , as it is predicted to be a fingerprint of quantum pumping in the JQEP [16]. After Φ -integration of I_{wire} , I_{wire}^A is therefore obtained as $I_{wire}^A = [I_{wire}(\Phi, I_{SQUID}) - I_{wire}(-\Phi, I_{SQUID})]/2$. The result of this procedure is shown in Fig. 3a which displays I_{wire}^A versus Φ and I_{SQUID} at 250 mK. The Φ_0 periodicity joined with the antisymmetry imply that I_{wire}^A vanishes at $\Phi = \Phi_0/2$, while its sign and magnitude can be changed by varying Φ . Notably, I_{wire}^A is almost *symmetric* in I_{SQUID} . The theoretical I_{wire}^A calculated for the JQEP geometry through a dynamical scattering approach [23–25] assuming for the NW multiple independent modes is shown in Fig. 3b (see Supplementary Information). Although rather idealized, the model is an essential tool to predict the pumped current symmetries of the JQEP. Remarkably, summing over many NW modes yields I_{wire}^A which is almost symmetric in I_{SQUID} , in agreement with the experiment.

Figure 3c shows I_{wire}^A versus Φ and I_{SQUID} over a wider range of SQUID currents. Specifically, I_{wire}^A turns out to be a non-monotonic function of I_{SQUID} , initially increasing then being suppressed for large I_{SQUID} . This is emphasized in Fig. 3d where $I_{wire}^A(\Phi)$ is plotted for selected values of I_{SQUID} . I_{wire}^A is a sinusoidal-like function of Φ whose amplitude depends on I_{SQUID} , and is maximized at $\Phi \sim (1/4)\Phi_0$ and $\Phi \sim (3/4)\Phi_0$.

The full $I_{wire}^A(V_{SQUID})$ dependence for a few values of flux is displayed in Fig. 3e and highlights both the monotonic linear increase for low V_{SQUID} and suppression at large V_{SQUID} . The symmetry in V_{SQUID} (i.e., in I_{SQUID}) is emphasized as well. Furthermore, $|I_{wire}^A|$ is maximized at $|V_{SQUID}^{max}| \approx 0.4$ mV independently of Φ , where it reaches values exceeding 20 pA. By converting V_{SQUID}^{max} in terms of the Josephson frequency we get $\nu_J \simeq 190$ GHz whose corresponding time, $\nu_J^{-1} \sim 5$ ps, is comparable to $\tau_D = W^2/D \simeq 4$ ps, i.e., the time required by electrons to diffuse in the NW between the Josephson junctions. In the above expression $W \simeq 250$ nm is the width of the SQUID central electrode (Fig. 1b) which we assume to coincide with the separation between the weak-links, whereas $D \simeq 0.015$ m²/s is the diffusion coefficient of the NW [26]. The transition between the regime of I_{wire}^A enhancement as a function of V_{SQUID} to the one of I_{wire}^A suppression can be explained in terms of the ability of the electrons to follow adiabatically the time-dependent parameters up to a maximum frequency set by τ_D^{-1} . Another possible contribution to the suppression observed at larger V_{SQUID} might stem from weakening of the ac Josephson coupling at high applied current [27].

The $I_{wire}^A(V_{SQUID})$ dependence plotted over a reduced bias range is displayed in Fig. 3f. In particular, I_{wire}^A

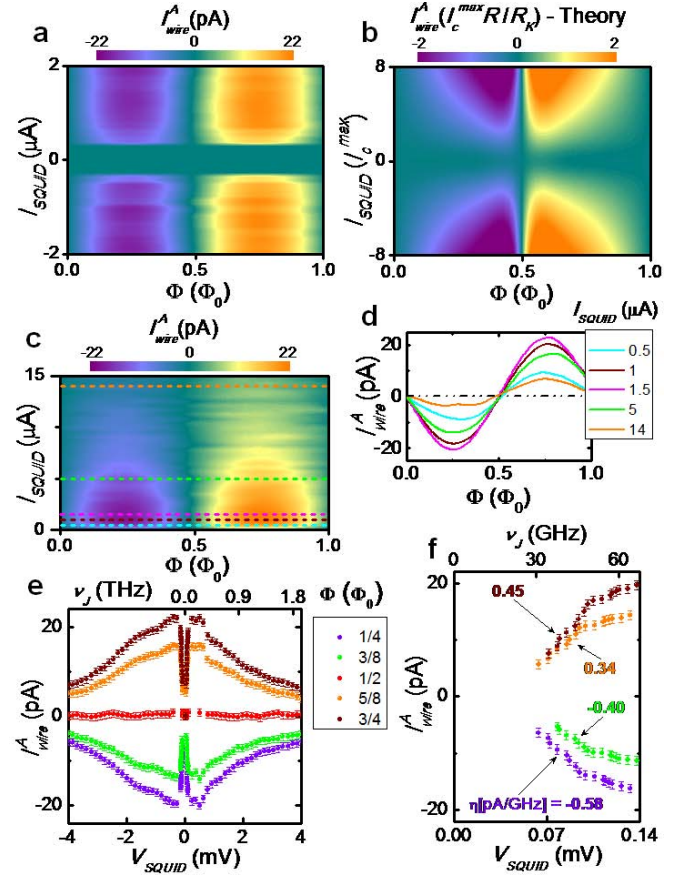


FIG. 3. Flux and I_{SQUID} dependence of the antisymmetric part of current flowing in the NW. (a) Color plot of I_{wire}^A versus I_{SQUID} and Φ . (b) Color plot of the theoretical zero-temperature I_{wire}^A versus I_{SQUID} and Φ . The calculation was performed for the JQEP geometry assuming the same asymmetry between the Josephson junctions as in the experiment. I_c^{max} is the sum of the critical currents of the two Josephson junctions, R is the total shunting SQUID resistance, and $R_K \simeq 25.8$ k Ω is the Klitzing resistance (see Supplementary Information for further details). (c) Color plot of I_{wire}^A versus I_{SQUID} and Φ shown over a wider range of I_{SQUID} . (d) I_{wire}^A versus Φ for a few representative values of I_{SQUID} . The latter are indicated as dashed lines of the same color in panel (c). (e) I_{wire}^A versus V_{SQUID} for a few selected values of Φ . (f) I_{wire}^A versus V_{SQUID} plotted over a smaller range of V_{SQUID} for the same Φ values as in panel (e). The slope in the linear regime, expressed in pA/GHz, is denoted with η . In (e) and (f) the error bars represent the standard deviation of the current values calculated over several measurements, and the upper horizontal scale is expressed in terms of the Josephson frequency ν_J . All measurements are taken at $T = 250$ mK.

shows a linear behavior with slope η which depends on the applied flux, and obtains values as high as several 10^{-1} pA/GHz. In the so-called ‘adiabatic regime’, i.e., where pumped current is expected to vary linearly with frequency, η would therefore correspond to some 10^{-3} electrons per pump cycle.

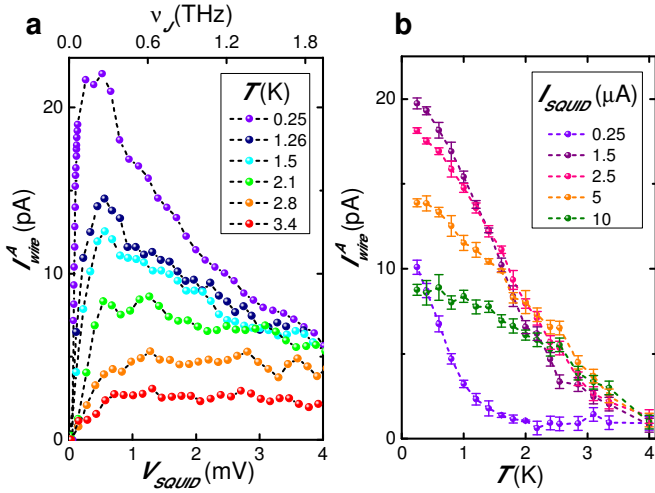


FIG. 4. **Temperature dependence of the antisymmetric part of the current flowing in the NW.** (a) I_{wire}^A versus I_{SQUID} measured at several bath temperatures T . (b) I_{wire}^A versus T at selected bias currents I_{SQUID} . Note the saturation of I_{wire}^A at low temperature as well as its suppression at high T . The error bars represent the standard deviation of the current values calculated over several measurements. Dashed lines in both panels (a) and (b) are guides to the eye, and all measurements are taken for $\Phi = (3/4)\Phi_0$.

The role of temperature (T) is shown in Fig. 4a which displays I_{wire}^A versus V_{SQUID} at $\Phi = (3/4)\Phi_0$ for several increasing temperatures. I_{wire}^A monotonically decreases upon increasing T , which can be ascribed to the influence of thermal smearing as well as thermal-induced dephasing, and is suppressed for $T \gtrsim 3.5$ K. We stress that the aforementioned temperature is substantially smaller than T_c , the latter setting the disappearance of both Josephson effect and superconductivity in the JQEP. The $I_{wire}^A(T)$ dependence at the same flux is shown in Fig. 4(b) for a few I_{SQUID} values. Specifically, I_{wire}^A begins to round off at lower temperatures indicating a saturation, whereas it is damped at higher T . Low-temperature behavior suggests that current tends to saturate upon reducing temperature when the “effective” separation between Josephson junctions becomes of the same order of the electron coherence length in the NW, $L_T = \sqrt{\hbar D / (2\pi k_B T)} \sim 270$ nm at 250 mK, where \hbar is the reduced Planck’s constant while k_B is the Boltzmann’s constant. By contrast, the decay of L_T at higher temperatures may be considered as one of the predominant decoherence mechanisms leading to I_{wire}^A suppression. Further study is needed to clarify this point.

It is worthwhile to emphasize that other effects which might manifest in the JQEP would yield currents characterized by symmetries markedly different from the ones predicted for quantum pumping (see Supplementary Information). Among these we recall (1) any spurious current due to asymmetry between the junctions which is

always dominated by a component symmetric in Φ and antisymmetric in I_{SQUID} ; (2) any thermocurrent generated by a different power dissipated in the two junctions, which is expected to be predominantly symmetric in both Φ and I_{SQUID} .

We finally note that other normal conductors than InAs NWs could be used for the implementation of the JQEP. This might pave the way to the investigation of the interplay between superconductivity-induced quantum pumping and exotic electronic states existing, for instance, in graphene [28] or in carbon nanotubes [29].

We gratefully acknowledge L. Faoro, R. Fazio, L. B. Ioffe, J. König, J. P. Pekola, V. Piazza, H. Pothier, and S. Russo for fruitful discussions, and D. Ercolani for providing the InAs nanowires. The work was partially supported by the NanoSciERA project “NanoFridge”. F.T acknowledges financial support from EU through the projects “SOLID” and “GEOMDISS”.

METHODS SUMMARY

Selenium doped InAs NWs were grown by chemical beam epitaxy on an InAs 111B substrate. Gold catalyst particles were formed by thermal dewetting (at 520° C for 20 min) of a 0.5-nm-thick Au film under TBA flux. NWs were grown for two hours at 420° C using TBA, TMI and DTBSe metallorganic precursors with line pressures of 2.0 Torr, 0.3 Torr, and 0.4 Torr, respectively. NWs have diameters of 90 ± 10 nm and are around 2.5 μ m long. Transport parameters were estimated over an ensemble of nominally identical 1 μ m-long NW field effect transistors using a charge control model [30] and a numerical evaluation of the gate capacitance. Carrier density was estimated to be $n = 1.8 \pm 0.8 \times 10^{19}$ cm $^{-3}$ and electron mobility $\mu = 300 \pm 100$ cm 2 /Vs. The devices were fabricated using a technique of dry cleavage of the NWs onto Si/SiO $_2$ substrates (500 nm oxide on intrinsic Si). Contacts were obtained by a two-step aligned process: thermal evaporation of Ti/Au (10/80 nm) was performed first and followed by electron-beam deposition of Ti/V (15/120 nm) in an UHV chamber [21]. InAs NWs were treated with a NH $_4$ S $_x$ solution before each evaporation step to get transparent metal-NW contacts [26].

The magneto-electric characterization of the devices was performed in a filtered 3 He refrigerator (two-stage RC- and π -filters) down to ~ 250 mK using a standard 4-wire technique. Current injection at the SQUID terminals was obtained by using a battery-powered floating source, whereas voltage and current were measured by room-temperature preamplifiers. Derivative measurements (flux-to-voltage as well as flux-to-current transfer functions) were performed with standard low-frequency lock-in technique by superimposing a small modulation to the applied magnetic field.

$$\phi_4 = \text{sign}(I_{SQUID})\omega_J t - \delta\varphi \quad (7)$$

$$\phi_5 = -\frac{\delta\varphi}{2} - \arctan\left[\frac{1}{r} \cot\left(\frac{\delta\varphi}{2}\right)\right] + \frac{\pi}{2}\text{sign}(\sin\frac{\delta\varphi}{2}) - \frac{\pi}{2}\text{sign}(I_{SQUID}), \quad (8)$$

where $\omega_J = 2\pi\nu_J = 2\pi|V_{SQUID}|/\Phi_0$ is the Josephson angular frequency and the function \arctan takes values between $-\pi/2$ and $\pi/2$. The value of ϕ_5 is chosen to ensure that the supercurrent is maximized in the limit of $\omega_J \rightarrow 0$. As a consequence of this, all observable quantities exhibit the standard Φ_0 periodicity. The pumping parameters are defined as $x_1(t) = \cos(\omega_J t)$ and $x_2(t) = \sin(\omega_J t)$ so that $\exp(i\phi_3) = x_1 + ix_2$, $\exp(i\phi_4) = (x_1 + ix_2)\exp(-i\delta\varphi)$. From this choice is clear that the two parameters are maximally out of phase, independently of $\delta\varphi$, and that the path is a circle of radius one centered around the origin. Since the N and S parts of the circuit have no common ground, the actual chemical potentials of the S electrodes with respect to the potential of the N electrodes have to arrange themselves so that no net current flows between the two parts of the circuit. As a consequence, the charge pumped per cycle can be written as

$$Q_p(\delta\varphi) = \frac{Q_1(\delta\varphi)G_2(\delta\varphi) - Q_2(\delta\varphi)G_1(\delta\varphi)}{G_1(\delta\varphi) + G_2(\delta\varphi)}, \quad (9)$$

where $G_i = |[S_{he}]_{i,1}|^2 + |[S_{he}]_{i,2}|^2$ is the conductance (in units of $e^2/\pi\hbar$) relative to lead i . Note that, in general, $Q_p(\delta\varphi)$ has no definite parity in $\delta\varphi$, in agreement with the results of Refs. [17, 18], and no definite parity in I_{SQUID} . The $\delta\varphi$ -antisymmetric component of the pumped current is obtained as $I_{wire}^A = (\omega_J/2\pi) [Q_p(\delta\varphi) - Q_p(-\delta\varphi)]/2$. In Fig. 3b I_{wire}^A is plotted in units of $I_c^{max}R/R_K$, where $I_c^{max} = I_{c1} + I_{c2}$ and $R_K = 2\pi\hbar/e^2$ is the Klitzing resistance. The current has been computed assuming that the NW carries 50 independent channels, each of which described by a scattering matrix obtained taking ψ_λ , q_λ and the phases accumulated along the two N wires as random parameters, while setting $\gamma_t = 1/10$, $\gamma_m = 1/11$ and $\gamma_b = 1/13$.

In the configuration where lead 1 is a voltage probe (rather than connected to ground) one can calculate the voltage V_p which develops at lead 1 as a consequence of the charge pumped. V_p , determined by setting to zero the current flowing in the NW, can be written as

$$V_p(\delta\varphi) = |V_{SQUID}(\delta\varphi)| \frac{G_1(\delta\varphi) + G_2(\delta\varphi)}{G_1(\delta\varphi)G_2(\delta\varphi)} Q_p(\delta\varphi). \quad (10)$$

The G_i has, in general, no definite parity in $\delta\varphi$ and I_{SQUID} . Furthermore, $\frac{G_1(\delta\varphi) + G_2(\delta\varphi)}{G_1(\delta\varphi)G_2(\delta\varphi)}$ is approximately even in both quantities also in the presence of a small asymmetry between the two Josephson junctions (which is typically the case of any realistic situation), so that V_p and Q_p show the same parity both in $\delta\varphi$ and I_{SQUID} .

The flux-antisymmetric component of V_p is defined as $V_{wire}^A(\delta\varphi) = [V_p(\delta\varphi) - V_p(-\delta\varphi)]/2$.

We shall further discuss the spurious effects which can occur in the presence of a shunting dissipative current across the Josephson weak-links. If the two Josephson junctions are not equal, a spurious voltage V_s (containing a constant and a time-oscillating component) arises in the NW between the beam splitters t and b in Fig. 5. This produces a current I_s in the NW that is not originated by quantum pumping. On the one hand, the current $I_{s,const}$ related to the constant component of V_s reverses by changing the sign of I_{SQUID} , in contrast to I_{wire}^A , and it is an even function of $\delta\varphi$. On the other hand, it turns out that the quantum rectified current $I_{s,rect}$ associated to the oscillating component of V_s has no definite parity both in $\delta\varphi$ and I_{SQUID} , similarly to Q_p of Eq. (9). However, $I_{s,rect}$ exists only in the presence of a finite $I_{s,const}$, since they have the same physical origin. Yet, $I_{s,rect}$ is smaller than $I_{s,const}$ because the amplitude of the oscillating components of V_s is set by I_c^{max} , whereas the constant component of V_s is proportional to V_{SQUID} . Therefore, the total spurious current is dominated by the component that is even in flux and odd in I_{SQUID} which would be detected, if present, in the transfer function \mathcal{I}_{wire} . Since the measured derivative signal \mathcal{I}_{wire} is almost flux-symmetric [see Fig. 2(c)], we can rule out the presence of $I_{s,const}$ and therefore of quantum rectification. We stress that even in the presence of a sizable $I_{s,const}$, our calculations predict I_{wire}^A to be typically several orders of magnitude larger than the flux-antisymmetric component of $I_{s,rect}$ (which is even in I_{SQUID}) thus fully dominating the measured signal.

In analogy, the current I_{SQUID} might produce a different power dissipated between points t and b in Fig. 5 leading to a thermocurrent flowing through the NW. Since V_s is dominated by its constant component, this thermocurrent would be almost *symmetric* both in $\delta\varphi$ and I_{SQUID} , in contrast to I_{wire}^A . In addition, there could be a small contribution to the thermocurrent due to the oscillating component of V_s which would have no definite parity both in I_{SQUID} and $\delta\varphi$. Since the power dissipated is proportional to V_s^2 such contribution to the thermocurrent is *a fortiori* negligible.

In conclusions, all the mechanisms envisioned above to produce a spurious dc current can be distinguished from quantum pumping by their parity with respect to magnetic flux Φ or bias current I_{SQUID} .

Supplementary data Here we present additional data for another JQEP device with nominally-identical geometry. Its essential parameters are the SQUID normal-state resistance of $\sim 187\Omega$ and the resistance of the Au/NW/Au line of $\sim 2.1\text{ k}\Omega$. The general behavior of this device is similar to that discussed in the main text although it is characterized by less symmetry between the two Josephson junctions. Figure 6 (a) displays the

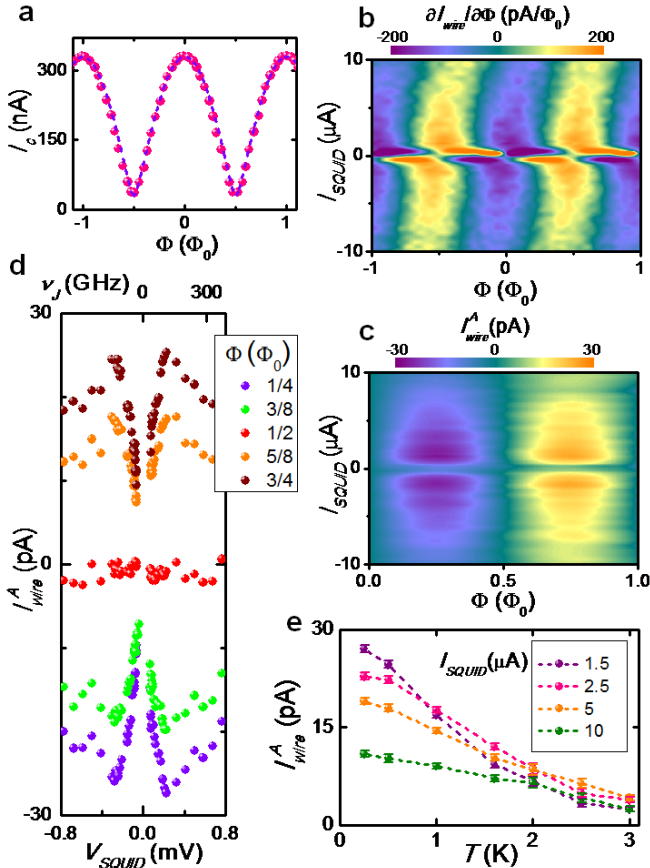


FIG. 6. **Experimental data for a different JQEP.** (a) Φ -dependent modulation of the SQUID critical current I_c . Dashed line is the theoretical behavior of a tunnel and resistively-shunted junction SQUID assuming an asymmetry $r \sim 9\%$ between the critical currents of the two weak-links. (b) Color plot of the NW flux-to-current transfer function $\mathcal{I}_{wire} = \partial I_{wire}/\partial \Phi$ versus Φ and I_{SQUID} . (c) Color plot of I_{wire}^A versus I_{SQUID} and Φ . (d) I_{wire}^A versus V_{SQUID} for a few selected values of Φ . Data in (a)-(d) are taken at $T = 250$ mK. (e) I_{wire}^A versus temperature T at selected bias currents I_{SQUID} for $\Phi = (3/4)\Phi_0$. The error bars represent the standard deviation of the current values calculated over several measurements, and dashed lines are guides to the eye.

full $I_c(\Phi)$ dependence of the SQUID measured at 250 mK which shows a maximum critical current of ~ 330 nA. Superimposed for a comparison (dashed line) is the model for a tunnel and resistively-shunted junction SQUID [22] assuming an asymmetry $r \sim 9\%$ between the critical currents of the two weak-links. The low-temperature flux-to-current transfer function $\mathcal{I}_{wire} = \partial I_{wire}/\partial \Phi$ versus Φ and I_{SQUID} is shown in Fig. 6b. \mathcal{I}_{wire} shows no definite parity both in Φ and I_{SQUID} which stems from the presence of a spurious current I_s in the NW, and might be attributed to the reduced symmetry of the SQUID junctions. Figure 6c shows the extracted I_{wire}^A versus Φ and I_{SQUID} at 250 mK which highlights both the non-monotonic dependence and symmetry in I_{SQUID} . The

full $I_{wire}^A(V_{SQUID})$ dependence for a few selected values of Φ at 250 mK is displayed in Fig. 6d, and emphasizes the overall symmetry in V_{SQUID} . For the present device $|I_{wire}^A|$ is maximized at $|V_{SQUID}^{max}| \approx 0.25$ mV where it obtains values exceeding ~ 27 pA. $|V_{SQUID}^{max}|$ corresponds to a Josephson frequency $\nu_J \simeq 120$ GHz (and related time $\nu_J^{-1} \sim 8$ ps). This difference from the device presented in the main text could originate from a slightly larger width W of the SQUID central electrode combined with a reduced NW diffusion constant which lead to an increased diffusion time τ_D . The $I_{wire}^A(T)$ dependence at $\Phi = (3/4)\Phi_0$ is shown in Fig. 6e for a few selected I_{SQUID} currents. Specifically, I_{wire}^A is rounded off at low temperature, whereas it is strongly damped and suppressed for $T \gtrsim 3$ K. The general behavior of I_{wire}^A and the arguments of the previous section therefore suggest that in this sample I_{wire}^A is fully dominated by quantum pumping, although a small component of quantum rectification might perhaps be present as well.

* f.giazotto@sns.it

- [1] D. J. Thouless, Phys. Rev. B **27**, 6083 (1983).
- [2] M. Büttiker, H. Thomas, and A. Prêtre, Z. Phys. B **94**, 133 (1994).
- [3] P. W. Brouwer, Phys. Rev. B **58**, R10135 (1998).
- [4] F. Zhou, B. Spivak, and B. Altshuler, Phys. Rev. Lett. **82**, 608 (1999).
- [5] H. Pothier, P. Lafarge, C. Urbina, D. Esteve, and M. H. Devoret, Europhys. Lett. **17**, 249 (1992).
- [6] J. M. Martinis, M. Nahum, and H. D. Jensen, Phys. Rev. Lett. **72**, 904 (1994).
- [7] N. E. Fletcher, J. Ebbecke, T. J. B. M. Janssen, F. J. Ahlers, M. Pepper, H. E. Beere, and D. A. Ritchie, Phys. Rev. B **68**, 245310 (2003).
- [8] J. Ebbecke, N. E. Fletcher, T. J. B. M. Janssen, F. J. Ahlers, M. Pepper, H. E. Beere, and D. A. Ritchie, Appl. Phys. Lett. **84**, 4319 (2004).
- [9] J. P. Pekola, J. J. Vartiainen, M. Möttönen, O.-P. Saira, M. Meschke, and D. V. Averin, Nature Phys. **4**, 120 (2008).
- [10] A. Fuhrer, C. Fasth, and L. Samuelson, Appl. Phys. Lett. **91**, 052109 (2007).
- [11] M. R. Buitelaar, V. Kashcheyevs, P. J. Leek, V. I. Talyanskii, C. G. Smith, D. Anderson, G. A. C. Jones, J. Wei, and D. H. Cobden, Phys. Rev. Lett. **101**, 126803 (2008).
- [12] B. Kaestner, V. Kashcheyevs, G. Hein, K. Pierz, U. Siegner, and H. W. Schumacher, Appl. Phys. Lett. **92**, 192106 (2008).
- [13] M. Switkes, C. M. Marcus, K. Campman, and A. C. Gosard, Science **283**, 1905 (1999).
- [14] P. W. Brouwer, Phys. Rev. B **63**, 121303(R) (2001).
- [15] L. DiCarlo, C. M. Marcus, and J. S. Harris, Jr., Phys. Rev. Lett. **91**, 246804 (2003).
- [16] S. Russo, J. Tobiska, T. M. Klapwijk, and A. F. Morpurgo, Phys. Rev. Lett. **99**, 086601 (2007).
- [17] T. A. Shutenko, B. L. Altshuler, and I. L. Aleiner, Phys. Rev. B **61**, 10 366 (2000).

- [18] M. Moskalets and M. Büttiker, Phys. Rev. B **72**, 035324 (2005).
- [19] A. F. Andreev, Sov. Phys. JETP **19**, 1228 (1964).
- [20] F. Giazotto, J. T. Peltonen, M. Meschke, and J. P. Pekola, Nature Phys. **6**, 254 (2010).
- [21] P. Spathis, S. Biswas, S. Roddaro, L. Sorba, F. Giazotto, and F. Beltram, Nanotechnology **22**, 105201 (2011).
- [22] M. Tinkham, *Introduction to Superconductivity, 2nd Edition* (McGraw-Hill, Inc., New York, 1996).
- [23] J. Wang, Y. Wei, B. Wang, and H. Guo, Appl. Phys. Lett. **79**, 3977 (2001).
- [24] M. Blaauboer, Phys. Rev. B **65**, 235318 (2002).
- [25] F. Taddei, M. Governale, and R. Fazio, Phys. Rev. B **70**, 052510 (2004).
- [26] S. Roddaro, A. Pescaglini, D. Ercolani, L. Sorba, F. Giazotto, and F. Beltram, Nano Res. (2011) (in print).
- [27] R. E. Harris, Phys. Rev. B **10**, 84 (1974).
- [28] A. H. Castro Neto, F. Guinea, N. M. R. Peres, K. S. Novoselov, and A. K. Geim, Rev. Mod. Phys. **81**, 109 (2009).
- [29] Y. Wei and J. Wang, Phys. Rev. B **66**, 195419 (2002).
- [30] X. Jiang, Q. Xiong, S. Nam, F. Qian, Y. Li, and C. M. Lieber, Nano Lett. **7**, 3214 (2007).